ELSEVIER

Journal of Power Sources 109 (2002) 111–120

JOURNAL OF POWER SOURCES

www.elsevier.com/locate/jpowsour

Modelling of simple hybrid solid oxide fuel cell and gas turbine power plant

S.H. Chan*, H.K. Ho, Y. Tian

Fuel Cell Strategic Research Programme, School of Mechanical and Production Engineering, Nanyang Technological University, 50 Nanyang Avenue, Singapore 639798, Singapore

Received 26 October 2001; accepted 17 January 2002

Abstract

This paper presents the work on a simple, natural gas-fed, hybrid solid oxide fuel cell–gas turbine (SOFC–GT) power-generation system. The system consists of an internal-reforming SOFC (IRSOFC) stack, a combustor, a GT, two compressors and three recuperators. Two case studies are conducted with particular attention on the effects of operating pressure and fuel flow-rate on the performance of the components and overall system. Results show that an internal-reforming hybrid SOFC–GT system can achieve an electrical efficiency of more than 60% and a system efficiency (including waste heat recovery for co-generation) of more than 80%. It is also found that increasing the operating pressure will improve the system efficiency, whereas increasing the fuel flow-rate (while keeping the fuel utilisation rate unchanged) causes the system efficiency to decrease. In the latter case, the increase in system fuel consumption is relatively higher which removes the benefit of increase in SOFC stack and turbine power output.

Keywords: Natural gas; Hybrid system; Gas turbine; Solid oxide fuel cell; Power plant

1. Introduction

The demand for power-generation systems of high efficiency and with low emission is of increasing importance. Fuel cells, as alternatives to conventional energy-conversion systems, have the prospect for exploiting fossil fuels more benignly and efficiently. The various types of fuel cells symbolise quite different technologies, with no clear winner to-date [1]. Nevertheless, the high-temperature solid oxide fuel cell (SOFC) appears better suited to power generation in a hydrocarbon fuel economy. Moreover, due to the synergistic effects, hybrid SOFC and gas turbine (GT) technology has been identified to be a superior power-generation technology to many other options. Predicted results shown that the integration into a more complex GT cycle of a pressurised SOFC which is multi-stage, inter-cooled, reheated and recuperated, can result in an electrical efficiency of 70% or higher (net ac per lower heating value (LHV) of fuel) can be expected [2–4]. For small-scale, electrical power-generation systems consisting of advanced microturbines and SOFC stacks, with a power rating of 250 kW, an electrical efficiency of 65% (net ac per LHV of fuel) can be expected [5]. Other advanced system studies, which include thermo-economic assessment of internal-reforming SOFC (IRSOFC)–GT combined cycles and take into account several technological constraints, have also been reported in detail [6].

In this investigation, attention is focused on the development of a model for a simple natural gas-fed, hybrid SOFC–GT power-generation system. The model is based on the first law of thermodynamics. The IRSOFC stack, which is the heart of the system, interacts with other system components and causes a complicated interdependency between them. Thus, it is useful to consider all performance-related parameters as a function of the thermodynamic states, e.g. to relate the exchange current density of the fuel cell and resistivities of cell components to the temperature of the SOFC stack. A general-purpose mathematical software tool, MATLAB, is adopted to develop the simulation code.

2. System configuration and description

The configuration of the hybrid SOFC–GT power-generation system is shown in Fig. 1. The system consists of an IRSOFC stack, a combustor, a GT and a power turbine (PT), two compressors, and three recuperators. An inverter (not shown) with a typical efficiency of 96.5% is considered. The mechanical work produced by the GT is used to drive

* Corresponding author. Tel.: +65-790-4862; fax: +65-791-1859.
E-mail address: mshchan@ntu.edu.sg (S.H. Chan).

0378-7753/02/$ – see front matter
PII: S0378-7753(02)00051-4

Nomenclature

A	constant
B	constant
c_p	specific heat at constant pressure (J/mol K)
E	cell potential (V)
E^0	reversible cell potential (V)
F	Faraday constant (96 487 C/mol)
G	Gibbs free energy (J/mol)
h	enthalpy (kJ/mol)
i	current density (mA cm^{-2})
i_0	exchange current density (mA cm^{-2})
i_L	limiting current density (mA cm^{-2})
K_p	equilibrium constant
n_i	molar flow-rate of specie i (kmol h^{-1})
p	pressure (bar)
Q	heat transfer (kJ)
Q_{rxn}	heat due to reactions (kJ)
Q_{surr}	heat loss to surroundings (kJ)
R	universal gas constant (8.314 J mol K)
R_i	ohmic resistance (Ω)
S	entropy (J mol K)
T	temperature (K)
U_f	fuel utilisation
Z	number of electrons participating in the reactions

Greek letters

β	transfer coefficient
δ	thickness (cm)
η_{Act}	activation polarisation (V)
η_{Conc}	concentration polarisation (V)
η_{Ohm}	ohmic overpotential (V)
ρ	resistivity (Ω m)

Subscripts

a	anode
c	cathode
r	reforming reaction
re	reversible
s	shifting reaction

the two compressors, and the sole mechanical power available for electrical power generation is derived from the PT.

Compressed fuel and air are preheated at their respective recuperators prior to entering the IRSOFC stack. Natural gas and oxygen are channelled through the anode and cathode compartments, respectively. Natural gas is internally reformed in the anode compartment and hydrogen-rich products are produced. The electrochemical reaction occurs at the three-phase boundaries (TPB) of both electrodes, and produces ionic flow through the electrolyte and electron flow across the electrodes. Electrical work (energy) is hence produced together with heat generation. The generated heat is partly dissipated to the environment, partly used to reform the natural gas, and partly used to heat up the feedstock and effluent gases. The high-temperature effluent gases of the IRSOFC stack, i.e. unutilised reformed natural gas and depleted air, are channelled to a combustor, where residual fuel (hydrogen, methane, carbon monoxide) reacts with the excess air. The amount of residual fuel in the exit of the SOFC stack is determined by the operating conditions of the IRSOFC.

The combusted fuel–air mixture then flows through the GT whereby mechanical power is produced. The produced power is consumed by the compressors which being the fuel and air to their required pressures. Subsequent expansion through the PT produces additional mechanical power which is used to generate the electrical power. The effluent gases exiting from the PT pass through a series of three recuperators where preheating of fuel and air occurs. Recuperator 3 is used for general heating purpose similar to that in a co-generation plant. For example, it heats liquid water from 25 to 90 °C for industrial processes.

3. System modelling

3.1. Internal reformer model

For a natural gas fuelled, hybrid SOFC–GT system, either internal or external reforming is needed. To reduce the expense of an external reformer and to provide additional 'cooling' for the SOFC stack, the use of an internal reformer is the better choice.

In the reforming process, steam is needed and can be obtained by vapourising the feed-water using the waste heat from the SOFC stack. The reaction mechanisms for the internal reforming of SOFC stack are:

$$x = CH_4 + H_2O \rightarrow CO + 3H_2 \quad \text{(reforming)} \tag{1}$$

$$y = CO + H_2O \rightarrow CO_2 + H_2 \quad \text{(shifting)} \tag{2}$$

$$z = H_2 + \tfrac{1}{2}(O_2) \rightarrow H_2O \quad \text{(electrochemical)} \tag{3}$$

where x, y and z indicate the respective molar flow-rate in the reaction. The equilibrium constants of reforming and shifting processes are temperature dependent and can be obtained from the following equation:

$$\log K_p = AT^4 + BT^3 + CT^2 + DT + E \tag{4}$$

where constants A, B, C, D and E are listed in Table 1 [6,7].

Table 1
Values of equilibrium constants of reforming and shifting processes

	Reforming	Shifting
A	-2.63121×10^{-11}	5.47301×10^{-12}
B	1.24065×10^{-7}	-2.57479×10^{-8}
C	-2.25232×10^{-4}	4.63742×10^{-5}
D	1.95028×10^{-1}	-3.91500×10^{-2}
E	-6.61395×10^{1}	1.32097×10^{1}

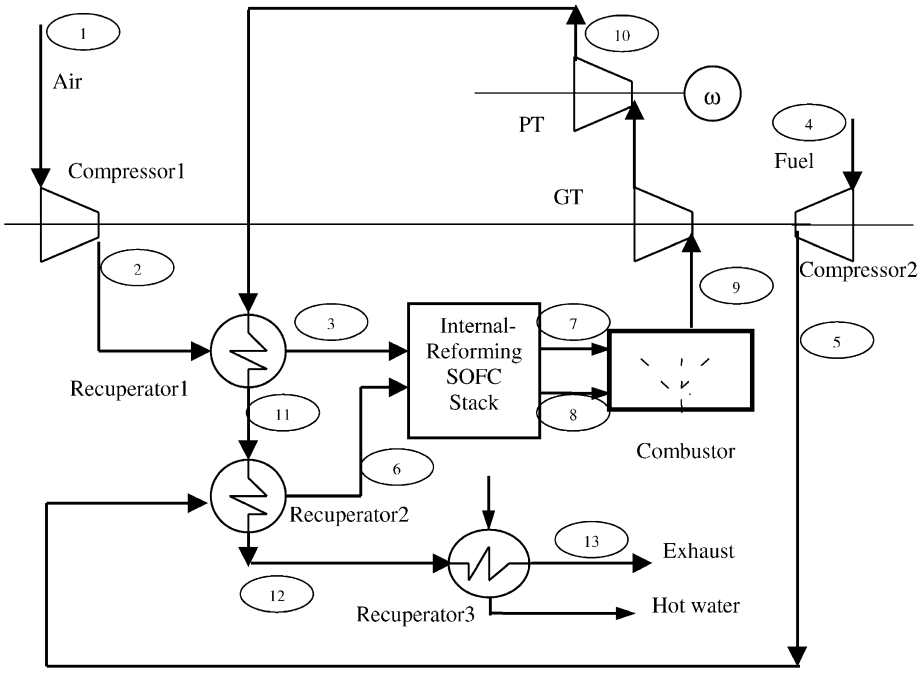

Fig. 1. Schematic of recuperated internal-reforming hybrid SOFC–GT system.

Assuming that the reforming and shifting reactions are always in equilibrium, the equilibrium constants can also be calculated from the partial pressures of the reactants and products, i.e.

$$K_{pr} = \frac{p_{H_2}^3 p_{CO}}{p_{CH_4} p_{H_2O}} \quad \text{(reforming)} \tag{5}$$

$$K_{ps} = \frac{p_{H_2} p_{CO_2}}{p_{CO} p_{H_2O}} \quad \text{(shifting)} \tag{6}$$

Assuming that x, y and z are the molar flow-rates of CH_4, CO and H_2, respectively, participating in the reactions, then:

$$K_{pr} = \frac{([CO]^i + x - y)/(n_{tot}^i + 2x)([H_2]^i + 3x + y - z)/(n_{tot}^i + 2x)}{([CH_4]^i - x)/(n_{tot}^i + 2x)([H_2O]^i - x - y + z)/(n_{tot}^i + 2x)} p_{cell}^2 \tag{7}$$

$$K_{ps} = \frac{([CO_2]^i + y)/(n_{tot}^i + 2x)([H_2]^i + 3x + y - z)/(n_{tot}^i + 2x)}{([CO]^i + x - y)/(n_{tot}^i + 2x)([H_2O]^i - x - y + z)/(n_{tot}^i + 2x)} \tag{8}$$

$$z = U_f(3x + y) \tag{9}$$

where superscript i is inlet; U_f fuel utilisation rate; n_{tot}^i total inlet molar flow-rate (or $n_{NG} + n_{H_2O}$).

When the temperature is known, the equilibrium constants can be calculated from Eq. (4) and the unknown x, y and z are determined by solving the simultaneous Eqs. (7)–(9) at the given fuel utilisation rate and inlet conditions of the flow.

Both the reforming and shifting reactions are endothermic; the heat needed for each reaction can be calculated from Eqs. (10) and (11), respectively, i.e.

$$Q_r = x(h_{CO} + 3h_{H_2} - h_{H_2O} - h_{CH_4}) \tag{10}$$

$$Q_s = y(h_{CO_2} + h_{H_2} - h_{CO} - h_{H_2O}) \tag{11}$$

Assuming that the heat generated from the electrochemical process of the fuel cell stack is Q_{rxn}, the total heat available for transfer from the stack will be:

$$Q = Q_{rxn} - Q_r - Q_s \tag{12}$$

3.2. SOFC model

The fuel cell model developed in this study is based on a tubular design and is fed by the natural gas, though it can be customised to accept different types of fuel cell designs and feedstock. The geometric and performance related data of the SOFC are based on the design developed by Siemens–Westinghouse [8]. To simplify the study, this model focuses on the thermodynamic aspect and the associated electrochemical processes of the cell operation. Treating all the cells as identical, the performance of the stack can be estimated. Hence, knowing the amount of fuel consumed by the stack, the total current produced by the stack can be calculated; while the cell voltage can be determined based on information for the stack temperature and the fuel utilisation rate. With known cell voltage and the total current, the electrical power of the stack is calculated.

For a H_2–O_2 reaction in a SOFC with known partial pressures of reactants and products, the ideal reversible cell potential can be calculated from the Nernst equation, i.e.

$$E_{\mathrm{re}} = E^0 + \Delta E = \frac{-\Delta G^0}{nF} + \frac{-\Delta G}{nF} = \frac{-\Delta G^0}{2F} + \frac{RT}{2F}\ln\frac{p_{\mathrm{H_2}}p_{\mathrm{O_2}}^{1/2}}{p_{\mathrm{H_2O}}} \tag{13}$$

There are several sources, however, which contribute to the irreversible losses in an operating fuel cell. These losses, usually termed polarisation, overpotential or overvoltage (η), originate primarily from three sources, namely: (i) activation overpotential (η_{Act}); (ii) ohmic overpotential (η_{Ohm}); and (iii) concentration overpotential (η_{Conc}). Hence, the actual potential of an operating fuel cell will be in the form of:

$$E = E_{\mathrm{re}} - (\eta_{\mathrm{Act}} + \eta_{\mathrm{Ohm}} + \eta_{\mathrm{Conc}}) \tag{14}$$

where

$$\eta_{\mathrm{Act}} = f^{-1}\left(\frac{i}{i_0(T)}\right) \quad \text{or} \quad \frac{i}{i_0(T)} = \left\{\exp\left(\beta\frac{F\eta_{\mathrm{Act}}}{RT}\right) - \exp\left(-(1-\beta)\frac{F\eta_{\mathrm{Act}}}{RT}\right)\right\}$$

$$\eta_{\mathrm{Ohm}} = i\sum_j R_j = i\sum_j \frac{A_j\,\mathrm{e}^{B_j/T}\delta_j}{A_{\mathrm{s},j}}$$

$$\eta_{\mathrm{Conc}} = \left(\frac{RT}{nF}\right)\ln\left(1 - \frac{i}{i_{\mathrm{L}}}\right)$$

where β is the transfer coefficient; i_0 is the apparent exchange current density; $\sum R_j$ is the total cell resistance, which includes electronic and ionic resistance; A_j and B_j are constants specific to the materials used; δ_j is the thickness of the respective cell component; i_{L} is the limiting current density.

3.3. SOFC stack model

The SOFC stack consists of a series of many single cells in order to increase the voltage output and hence the electrical power for practical applications. Since the SOFC stack interfaces with many other system components, depending on what the system configuration is, its performance will be closely related to the thermodynamic states of the components to which it is connected.

To calculate the stack temperature, three heat sources/sinks should be determined; namely: (i) heat generated due to the electrochemical reaction in the SOFC stack; (ii) heat consumed by internal reforming; (iii) heat loss to the surroundings.

The heat generated by electrochemical reaction comes from two main sources. One is due to the reversible reaction, while the other is due to the process irreversibility associated with cell polarisation. The reaction heat takes the form of:

$$Q_{\mathrm{rxn}} = i\sum\eta + T\,\Delta S \tag{15}$$

$$\Delta S = \left(S^0_{\mathrm{H_2O}} - S^0_{\mathrm{H_2}} - \frac{1}{2}S^0_{\mathrm{O_2}}\right) - \frac{R}{2}\ln\left(\frac{p^2_{\mathrm{H_2}}p_{\mathrm{O_2}}}{p^2_{\mathrm{H_2O}}}\right)$$

where η and ΔS are both temperature dependent.

Under steady-state operation of a SOFC stack, the heat generated by the electrochemical reaction will provide the heat for internal reforming and will heat up the mixture of products and non-reacted residual gases. By applying the steady flow energy equation and assuming that the amount of heat dissipated to the surroundings is Q_{surr} and the effluent gases from the anode and cathode exits are well mixed and arrive at temperature T_2, then:

$$Q = Q_{\mathrm{surr}} + \Delta h_{\mathrm{c1}} + \Delta h_{\mathrm{c2}} + \Delta h_{\mathrm{a1}} + \Delta h_{\mathrm{a2}} \tag{16}$$

where Δh_{c1}, Δh_{a1} are the enthalpy changes of reactants at the cathode and anode, respectively; Δh_{c2}, Δh_{a2} are the enthalpy changes of products at the cathode and anode, respectively.

Given

$$\Delta h = \int_{T_1}^{T_2} c_p\,\mathrm{d}T \tag{17}$$

and combining Eqs. (12), (16) and (17), then:

$$\begin{aligned} Q' &= Q_{\mathrm{rxn}} - Q_{\mathrm{r}} - Q_{\mathrm{s}} - Q_{\mathrm{surr}} \\ &= \left(n_1\int_{T_{1\mathrm{a}}}^{T_2} c_p\,\mathrm{d}T\right)_{\mathrm{r}} + \left(n_2\int_{T_{1\mathrm{a}}}^{T_2} c_p\,\mathrm{d}T\right)_{\mathrm{p}} \\ &\quad + \left(n_3\int_{T_{1\mathrm{c}}}^{T_2} c_p\,\mathrm{d}T\right)_{\mathrm{r}} + \left(n_4\int_{T_{1\mathrm{c}}}^{T_2} c_p\,\mathrm{d}T\right)_{\mathrm{p}} \end{aligned} \tag{18}$$

where n_1, n_2, n_3 and n_4 are the corresponding molar flow-rates of the gases.

Since specific heat c_p is also a function of temperature, it is fitted to a second order polynomial of the temperature function and is integrated across a temperature span of T_1 and T_2. In this study, the SOFC stack is assumed to be in thermal equilibrium with the effluent gases. Thus, the SOFC stack effluent gas temperature T_2 can be determined by the iterative computation. The iterations continue until the error between two successive calculations is less than the assigned tolerance. The error to meet the convergence criteria is given as:

$$Q_{\mathrm{error}} = \left|\frac{Q' - (Q_{\mathrm{rxn}} - Q_{\mathrm{r}} - Q_{\mathrm{s}} - Q_{\mathrm{surr}})}{Q_{\mathrm{rxn}} - Q_{\mathrm{r}} - Q_{\mathrm{s}} - Q_{\mathrm{surr}}}\right| < 1\% \tag{19}$$

3.4. Other system component models

Other system components that also play crucial roles in determining the overall performance of the plant include the compressors, turbines, recuperators and combustor. In this study, it is assumed that all system components are working at their respective designed conditions under steady-state operation. A set of operating parameters and the assumed efficiencies/effectiveness of these system components are given in Table 2. In addition, the initial states of the working fluids have to be assumed, in particular for the recuperators

Table 2
Setting/assumed values of performance-related parameters

Parameter	Setting/assumed value
Compressor isothermal efficiency	85%
Recuperator effectiveness	0.80
Recuperator pressure drop	1%
GT mechanical efficiency	99%
PT isentropic efficiency	85%
Inverter efficiency	96.5%
Generator efficiency	97%
SOFC length	50 cm
SOFC surface area	270 cm^2
Combustor isentropic efficiency	95%
Limiting current density	350 mA cm^{-2}
Electrolyte resistivity constants	$A = 0.00294$, $B = 10\,350$
Electrolyte thickness	0.004 cm
Interconnect resistivity constants	$A = 0.1256$, $B = 4690$
Interconnect thickness	0.01 cm
Cathode resistivity constants	$A = 0.00811$, $B = 600$
Cathode thickness	0.200 cm
Anode resistivity constants	$A = 0.00298$, $B = -1392$
Anode thickness	0.015 cm
Stack pressure drop	2%
Area ratio of cathode to anode	10

as the hot fluid temperatures (for example, the flow temperature at the exit of the PT) are not available at the beginning of the simulation. These assumed initial values, however, will converge after a few loops of iteration until the converging criteria are met. Computation of the heat-exchange between the hot and cold fluids in the recuperators, which are counter-flow heat exchangers, is based on the effectiveness-number of transfer units (ε-NTU) method.

4. Overpotentials in SOFC

4.1. Activation overpotential

The activation overpotential at different operating temperatures using the Butler–Volmer equation is shown in Fig. 2. The results show that the activation overpotential increases with increase in current density, but decreases with increase in temperature. It is obvious that the activation overpotential is zero at zero current density, which can never be the case if the Tafel equation is used. The latter yields an unreasonable activation overpotential of $-((\overline{R}T)/(4\beta F))\ln i_0$ at zero current density.

4.2. Ohmic overpotential

The ohmic resistance of the various cell components at different temperatures is shown in Fig. 3. It is obvious that, based on data for the Siemens–Westinghouse SOFC, the interconnector contributes the most to the overall ohmic resistance, and is followed by the electrolyte. The ohmic resistance of the electrodes, by comparison, contributes negligible overall ohmic resistance in the SOFC. Note that,

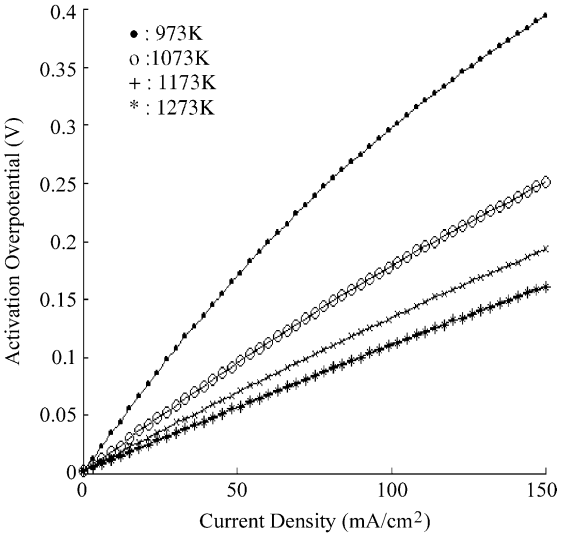

Fig. 2. Effect of temperature on activation overpotential.

the resistance of each component is determined not only by the respective resistivity but also by the thickness. It can be deduced that improved performance of the SOFC can be expected if a cell component of low resistivity is used as the support/substrate of SOFC. The resistance increases exponentially with decrease in temperature and this result in deteriorated fuel cell performance at undesirable low-temperature operation.

4.3. Concentration overpotential

The effect of the temperature on the concentration overpotential is given in Fig. 4. It can be seen that there is a significant increase in concentration overpotential when the operation of SOFC approaches the limiting current density of 345 mA cm^{-2}. More work can be done in the future to

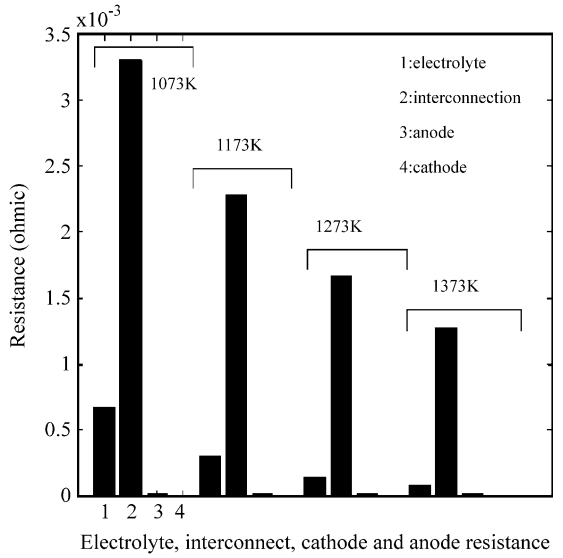

Fig. 3. Effect of temperature on ohmic resistance.

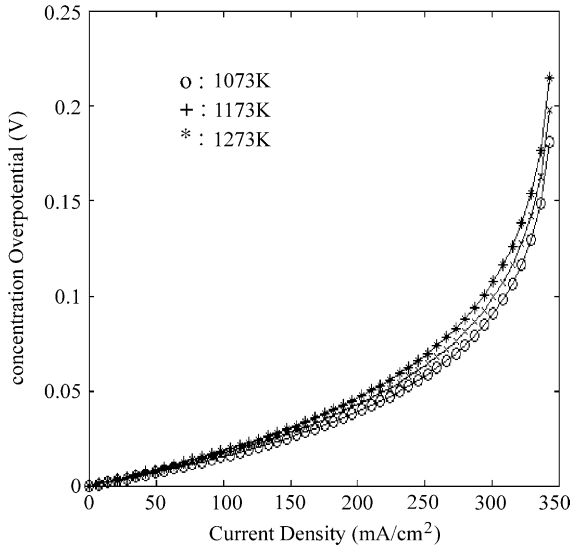

Fig. 4. Effect of temperature on concentration overpotential.

relate the effect of the fluid properties on the limiting current density or to use a more generalised polarisation model [9]. Normally, fuel cells are designed to operate slightly lower than the current density that corresponds to the peak power for a good compromise between the cell efficiency and operational stability. Hence, under normal operating conditions the present model is still applicable, as the concentration overpotential is not the rate-limiting factor.

5. Hybrid IRSOFC–GT system simulation

5.1. System performance simulation results

The pressure, temperature, gas flow-rate and composition at each node of the system (refer to Fig. 1) are listed in Tables 3 and 4. In this particular case study, the pressure ratio of both compressors is set to 9, the air flow-rate to 170 kmol h^{-1}, the fuel flow-rate to 15 kmol h^{-1}, and the fuel utilisation rate to 0.8. The total number of tubular SOFCs used in all cases is 60 000.

Table 3
Fluid properties for recuperated hybrid IRSOFC–GT power system

	Pressure (bar)	Temperature (K)	Gas flow-rate (kmol h^{-1})	Gas composition (%)
1	1	300	170	N_2: 79, O_2: 21
2	9	562	168.3	N_2: 79, O_2: 21
3	8.3	960	166.6	N_2: 79, O_2: 21
4	1	300	15	CH_4: 97, CO_2: 1.5, N_2: 1.5
5	9	562	14.85	CH_4: 97, CO_2: 1.5, N_2: 1.5
6	8.55	746	14.7	CH_4: 97, CO_2: 1.5, N_2: 1.5
7	7.64	1166	145.2	Refer to Table 4, cathode
8	7.65	1166	68.18	Refer to Table 4, anode
9	6.46	1466	206.34	Refer to Table 4, combustor
10	1.41	1061	204.3	Refer to Table 4, combustor
11	1.39	791.5	202.3	Refer to Table 4, combustor
12	1.36	773.4	200.2	Refer to Table 4, combustor
13	1.34	393	198.2	Refer to Table 4, combustor

Table 4
Gas composition at different nodes of the system

Gas composition						
H_2	O_2	N_2	H_2O	CO_2	CH_4	CO
Stack outlet (anode) (%)						
15.69	0	0.32	62.75	16.19	0.06	4.99
Stack outlet (cathode) (%)						
0	9.36	90.64	0	0	0	0
Combustor outlet						
0	3	64	26	7	0	0

Some results relating to cell and system performance, as well as the conditions at the exhaust (node 13), are extracted from the simulation and listed in Table 5. The cells operate at power density of 104.5 mW cm^{-2} at current density of 141.6 mA cm^{-2}, which is far away from the limiting current density of 345 mA cm^{-2}. The waste heat recovered from recuperator 3 is 731 kW with an exit flow temperature and a pressure of 393 K and 1.34 bar, respectively. Note that, the net electrical power output (ac) of the plant is 2105.25 kW, of which 381 kW comes from the PT. The latter contributes about 18% of the total electrical power output. The electrical and total efficiencies of the plant are 62.2 and 83.8%, respectively. The total (system) efficiency is defined as the ratio of the useful energy output to the LHV of the fuel; the former includes the electrical energy produced by the SOFC stack and the PT (in terms of ac power output), and the heat recovery at recuperator 3. Excluding the heat recovery in the calculation of useful energy output, the efficiency so obtained is defined as the electrical efficiency.

5.2. System performance under different operating pressures

The effect of operating pressure on stack temperature, cell voltage, stack and PT ac power outputs, waste heat recovery

Table 5
Cell and system performance related results from simulation

Cell voltage	0.738 V
Cell current density	141.6 mA cm^{-2}
Gas temperature at node 13	393 K
Gas pressure at node 13	1.34 bar
Stack temperature	1166 K
Compressor work (air side)	301 kW
Compressor work (fuel side)	26.6 kW
Net PT ac power output	381 kW
GT inlet temperature	1466 K
GT inlet pressure	6.46 bar
Waste heat recovery	731 kW
Electrical efficiency (LHV)	62.2%
Total efficiency (LHV)	83.8%

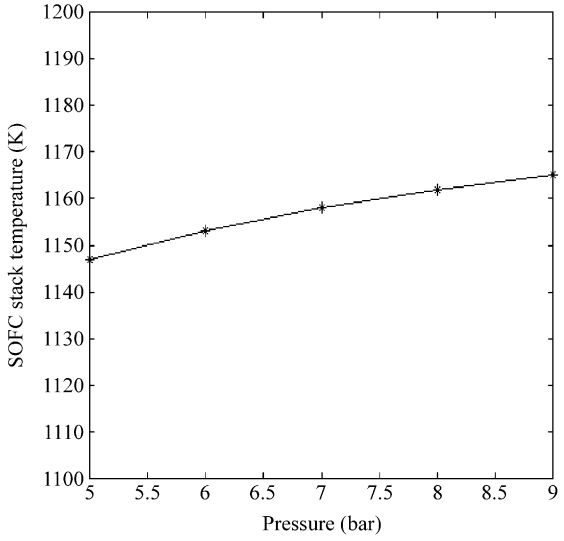

Fig. 5. Effect of flow pressure on stack temperature.

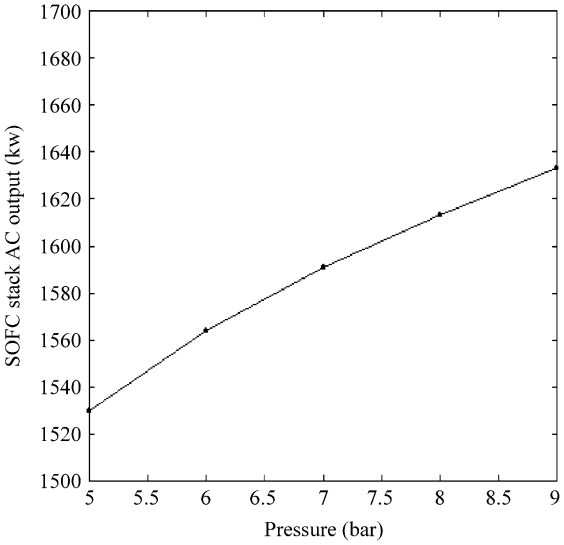

Fig. 7. Effect of flow pressure on stack ac power output.

and system efficiency is shown in Figs. 5–10, respectively. In this case study, the fuel and the air flow-rates are fixed at 15 and 170 kmol h^{-1}, respectively, with a 80% fuel utilisation rate. For simplicity, the pressures of the fuel and air are set to be the same, though they can be different under typical operational demand. Note that, the increase in fuel and air pressures through their respective compressors is associated with the increase in flow temperatures. This subsequently affects the operating temperature of the fuel cell through the thermal effect, and hence the overpotentials and heat generation. This means that the higher is the feedstock temperature, the higher will be the stack temperature. A higher stack temperature means, however, that the fuel cell operates more efficiently and less waste heat will be generated. The combined effect of flow enthalpies and heat generation in the fuel cells determines the final stack temperature.

The effect of operating pressure on the stack temperature is given in Fig. 5. As mentioned above, increase in operating pressure causes an increase in stack temperature. This makes the fuel cell operate more efficiently, which is reflected in increased cell voltage and stack ac power output, as shown in Figs. 6 and 7, respectively.

The increase in stack temperature implicitly means that there is also an increase in the exit flow temperature of the stack. Proportionally, both GT and PT would be able to produce more mechanical power through expansion processes with higher flow energy. The positive effect of flow pressure on the PT ac power output is demonstrated in Fig. 8.

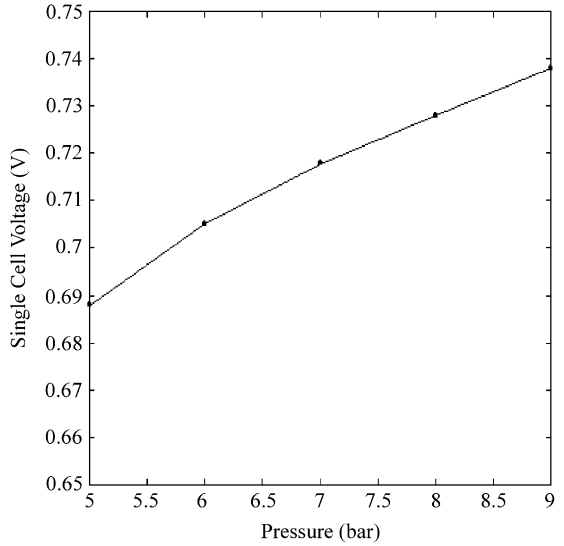

Fig. 6. Effect of flow pressure on cell voltage.

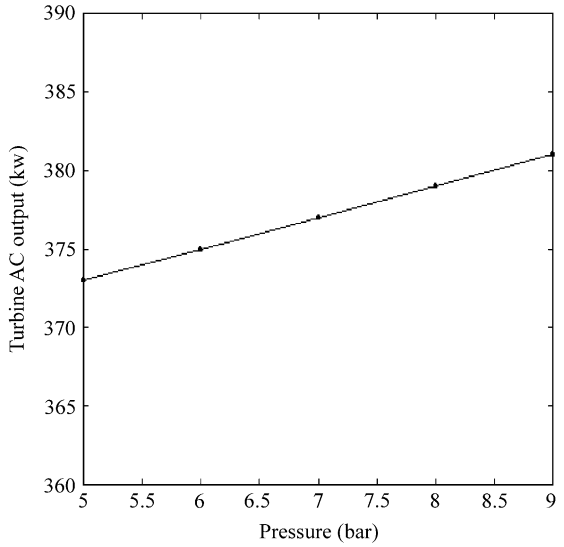

Fig. 8. Effect of pressure on turbine ac power output.

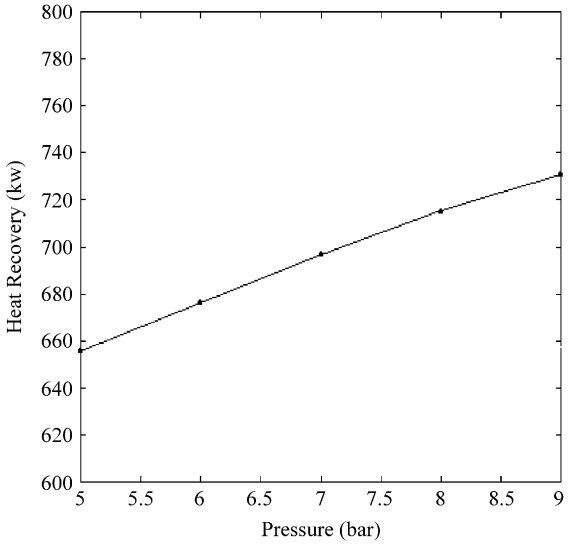

Fig. 9. Effect of pressure on heat recovery.

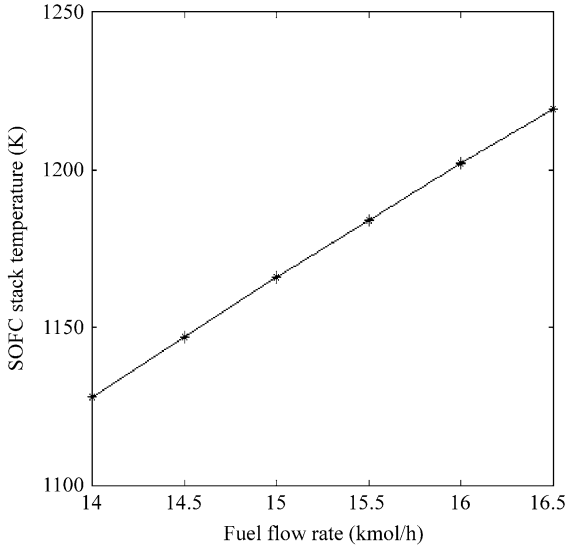

Fig. 11. Effect of fuel flow-rate on stack temperature.

Note that, the compressors and turbines are assumed to operate at their designed conditions and their respective efficiency is assigned with a constant value, though they should be varied with operating conditions. Provision has been made to use the characteristic maps to cater for various off-design operating conditions.

The effect of flow pressure on the heat recovery is presented in Fig. 9. The heat recovery is referred to the amount of energy that is obtainable from recuperator 3, which can be used to produce steam or hot water for industrial and commercial applications. As expected, more heat can be recovered from the higher operating pressure due to the higher flow temperature. The effect of flow pressure on the system efficiency is shown in Fig. 10. The simulation results indicate that although the increase in fuel and air pressures increases the work required by the compressors, the improvement in overall useful energy output outweighs this extra work required, and thus enhances the system efficiency.

5.3. System performance under different fuel flow-rates

The influence of fuel flow-rate on the stack temperature, cell voltage, stack and PT ac power outputs and system efficiency, is illustrated in Figs. 11–15, respectively. In this case study, the pressure ratios of the fuel and air compressors are fixed at 9, the air flow-rate at 170 kmol h^{-1} and fuel utilisation rate at 80%. With a constant fuel utilisation rate, a

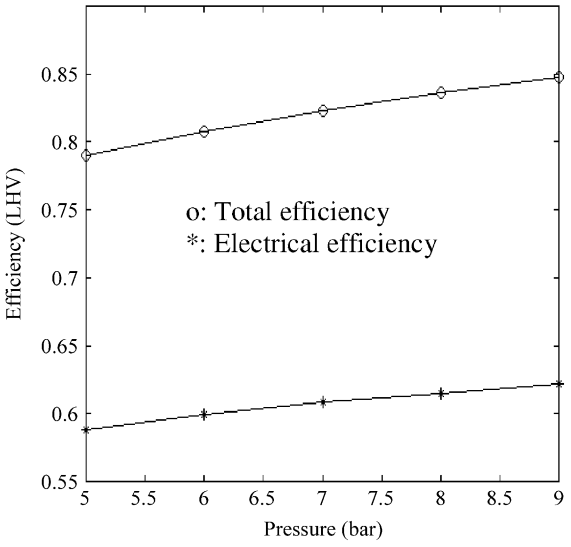

Fig. 10. Effect of pressure on system efficiency.

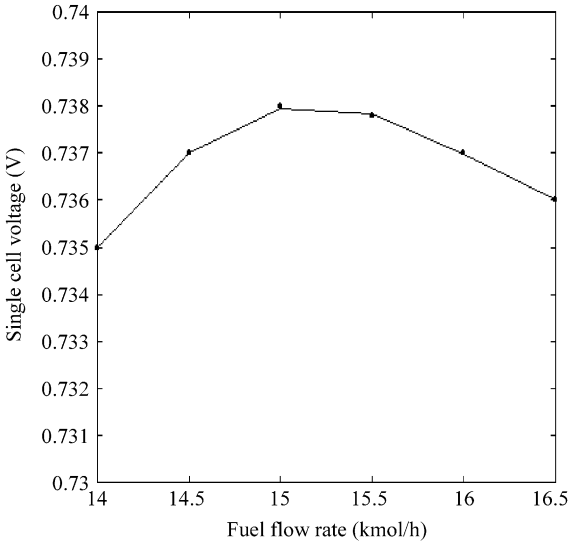

Fig. 12. Effect of fuel flow-rate on cell voltage.

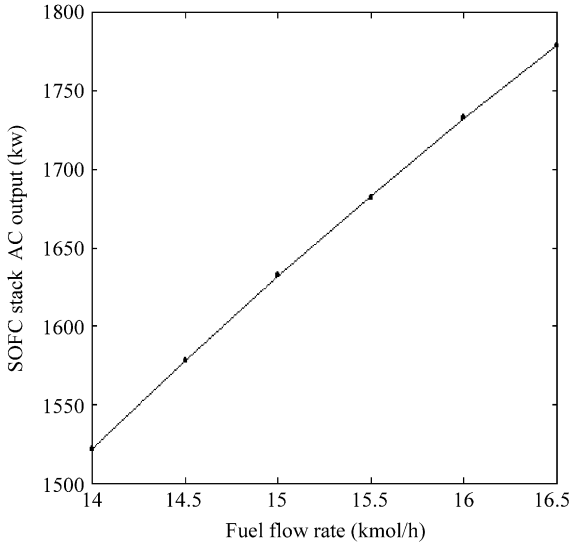

Fig. 13. Effect of fuel flow-rate on stack ac power output.

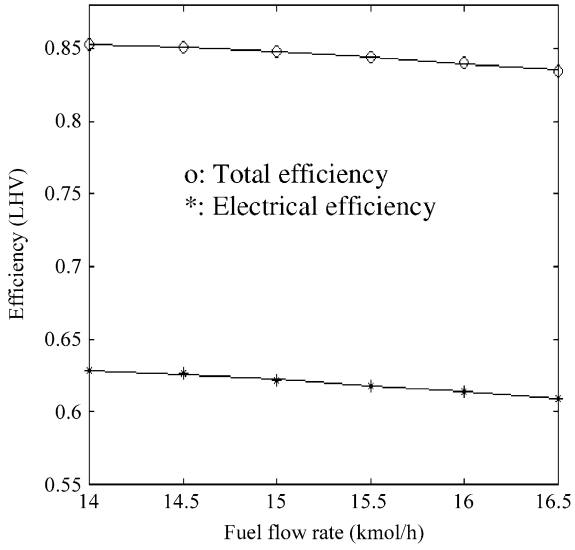

Fig. 15. Effect of fuel flow-rate on system efficiency.

higher rate of fuel flow means that more chemical energy is converted to electrical energy. Accordingly, more current will be produced and hence the current density is increased. This rise current/current density has a linear relationship with the amount of hydrogen consumed. The effect of fuel flow-rate on stack temperature is presented in Fig. 11. The higher the amount of current drawn from the SOFC stack, the higher will be the overall overpotential. This will increase the heat generation which, in turn, will raise the stack temperature.

The effect of fuel flow-rate on the cell voltage is given in Fig. 12. The combined effect of the increased stack temperature and current drawn has a significant impact on the cell performance. The former causes a reduced overall overpotential while the latter gives rise to an increased overall overpotential. In general, an increase in fuel flow-rate at constant fuel utilisation will produce an initial increase in cell voltage due to the stronger effect of the increased stack temperature on the overall overpotential. Then, the stronger effect of increased current density on overall overpotential assumes a dominant role and causes the cell voltage to fall.

The effect of fuel flow-rate on stack ac power output is shown in Fig. 13. Intuitively, an increase in fuel flow-rate causes an increase in current and thus raises the power output of the fuel cell stack. The power output due to the increase in current is partly offset by the drop of cell voltage at higher fuel flow-rates as can be seen in Fig. 12. Increase in stack temperature and gas flow-rate brings about the advantage of increased turbine power output, and thereby improves the turbine ac power output, as indicated in Fig. 14.

The system efficiency decreases with increasing the fuel flow-rate, as demonstrated in Fig. 15. Though there are increases in stack and turbine ac power outputs as well as heat recovery, the increase in fuel consumption causes a decline in system efficiency.

From this study, it can be seen that there is always a trade-off between the best efficiency and the highest power output of a thermodynamic system. For a specific SOFC technology, operation of the stack at higher efficiency would mean lower fuel consumption or higher capital cost (a greater number of fuel cells is needed). For a system to provide maximum power output, it is necessary to determine the fuel utilisation rate which corresponds to the current density that will yield the maximum power output.

On keeping the fuel flow-rate unchanged, an increase in fuel utilisation rate has a similar effect on system performance as that of increasing the fuel flow-rate. The increase in fuel utilisation rate would mean that more fuel is being

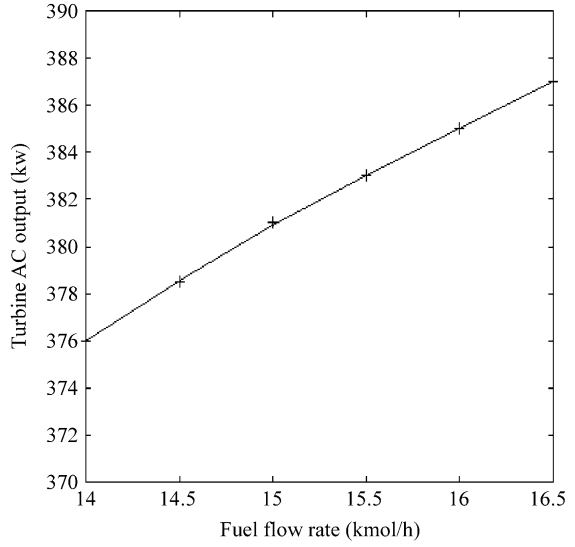

Fig. 14. Effect of fuel flow-rate on turbine ac power output.

consumed by the SOFC stack which causes a higher current density in the cell. The cell voltage decreases with increase in fuel utilisation, which is attributed to the increase in current density, as can be seen in a typical polarisation curve of cell potential versus current density.

6. Conclusions

A simple, natural gas-fed, hybrid SOFC power-generation system has been developed. The IRSOFC stack, which is the heart of the system, interacts with other system components and causes a complicated interdependency between them. Based on this simulation study, the following conclusions can be drawn.

(i) With the plant configuration under study, it is possible for a hybrid SOFC–GT power system to achieve an electrical efficiency greater than 60% and a system efficiency greater than 80%.
(ii) Given certain specific assumptions, an increase in operating pressure would have some positive impact on system efficiency, through improvements in cell efficiency, power output of the PT and waste heat recovery.
(iii) Keeping the fuel utilisation unchanged, the effect of fuel flow-rate on system efficiency, and vice versa, is not favourable. Though the power outputs of the stack and turbine show some improvement, the increase in system fuel consumption outweighs these advantages and causes a slight decrease in system efficiency.

References

[1] F.J. Gardner, M.J. Day, N.P. Brandon, M.N. Pashley, M. Cassidy, SOFC technology development at Rolls-Royce, J. Power Sources 86 (2000) 122–129.
[2] G.T. Lee, F.A. Sudhoff, Fuel cell/gas turbine system performance studies, in: Proceedings of the Fuel Cells 1996 Review Meeting, Department of Energy, FETC Publications, USA, 1996.
[3] S.E. Veyo, W.L. Lundberg, Solid oxide fuel cell power system cycles, ASME Paper 99-GT-356, 1999.
[4] D.J. White, Hybrid gas turbine and fuel cell systems—in perspective review, ASME Paper 99-GT-419, 1999.
[5] S. Campanari, Full load and part load performance prediction for integrated SOFC and microturbine system, J. Eng. Gas Turbines Power 122 (2000) 239–246.
[6] U.G. Bossel, Final report on SOFC data facts and figures, Swiss Federal Office of Energy, Berne, CH, 1992.
[7] A.F. Massardo, F. Lubelli, Internal reforming solid oxide fuel cell–gas turbine combined cycles (IRSOFC–GT). Part A. Cell model and cycle thermodynamic analysis, J. Eng. Gas Turbines Power 122 (2000) 27–35.
[8] N.F. Bessette II, W.J. Wepfer, Electrochemical and thermal simulation of a solid oxide fuel cell, Chem. Eng. Commun. 147 (1996) 1–15.
[9] S.H. Chan, K.A. Khor, Z.T. Xia, A complete SOFC polarization model and its sensitivity to the change of cell component thickness, J. Power Sources 93 (2001) 130.